MRS Communications

https://doi.org/10.1557/s43579-022-00191-8

MRS Communications

Research Letter

The effects of temperature, pressure, and time on lignin incorporation in bacterial cellulose materials

Jeremy L. Fredricks, Mallory Parker, PaulGrandgeorge, Andrew M. Jimenez, Esther Law, Marissa Nelsen, Eleftheria Roumeli, Materials Science and Engineering, University of Washington, Seattle, WA, USA

Address all correspondence to Eleftheria Roumeli at **eroumeli@uw.edu**

(Received 4 March 2022; accepted 20 May 2022)

Abstract

Due to the increasing detrimental impacts of mass non-renewable plastics over the last decades, cellulose-based materials have been extensively studied as a promising sustainable alternative. Here, we prepare lignocellulosic papers (LBC) from bacterial cellulose (BC) impregnated with lignin, and analyze their mechanical properties, microstructure, and wetting kinetics. We follow a design of experiment analysis to obtain the optimal pressing conditions of the BC and LBC papers, targeted at maximizing the specific ultimate tensile strength and toughness. At optimal conditions, lignin impregnation enhances the absolute modulus, strength, and toughness of BC by 108%, 142%, and 63%, respectively.

Introduction

Research into cellulose as a sustainable plastic alternative has continued to grow in the past few decades due to its inherent strength, abundance and ability to be readily extracted from renewable biomass and processed into new products.[1–7] Most commonly, cellulose is extracted from woody biomass, in a process that involves chemically stripping lignin and other cell wall components and subsequently processing the extracted cellulose.[1,6] Recently, however, studies have begun to focus on lignocellulosic materials, which take advantage of the upwards of 20% lignin present in the woody biomass for potential improvements in strength and hydrophobicity in the final product.[4,5]

The two different strategies which have been explored so far include the introduction of lignin as a filler in pure cellulose matrix materials, and the removal of other cell wall components from wood to leave a lignocellulose framework after chemical processing. The former strategy allows any type of cellulose to be used as a matrix, and as a result, it has been applied to introduce lignin in wood-extracted micro- and nano-cellulose blends.[4,8,9] Wang et al. recently demonstrated that heat-treating of cellulose-lignin blends, allows lignin to soften and fill the voids of the cellulose network, thus providing substantial improvements in mechanical properties and water stability of the composite.[4] Prior results from Jiang et al. concur with these observations and provide evidence that altering the hot-pressing temperature allows modulation of the mechanical properties of the lignocellulose composite.[9] Specifically, the reintroduction of lignin back into totally delignified cellulose matrices, at optimal press temperature (100–130°C), showed tensile strength in the composite to be five times higher compared to the conventional cellulose paper.[9] In another study, Farooq et al. introduced different amounts and types of lignin into nanofibrillated cellulose (from wood pulp) and reported a drastic improvement on the toughness of the composite in 10 wt% colloidal lignin particles. They also reported an increase in the stiffness of the composites at the expense of toughness when they hot-pressed their papers at 100°C.[10]

More recently, Xia et al. demonstrated the potential to create lignocellulose composites directly from woody biomass by selectively removing the other cell wall components and maintaining the native lignin-cellulose as found in cell walls.[5] That builds on a prior study by Song et al., who reported that partial wood delignification (via chemical treatment followed by hot-pressing) can lead to self-bonded composites with closed pore structures that achieve dramatically enhanced strengths, which are maximized at 10–15 wt% lignin.[11]

Another possibility for modifying properties of lignocellulose materials is by changing the cellulose source.[1,12] For example, a highly crystalline, pure cellulose nanofibrillar matrix can be naturally synthesized by certain types of bacteria in the form of a layered, interconnected stack of individual cellulose sheets (referred to as pellicle). Bacterial cellulose (BC) pellicles circumvent the unavoidable cellulose matrix partial degradation that occurs during delignifying chemical treatments of wood sources.[13]

Here, we aim to explore the effects of lignin in the mechanical properties of BC papers and understand how the processing conditions can enable tuning of the final obtained properties of the composite lignocellulose papers. We employ a design of experiment (DOE) analysis to facilitate a systematic understanding of the effects of lignin as well as the selected processing conditions and develop processing-structure–property relationships for the produced papers. Our detailed analysis revealed optimal processing temperature/pressure/time conditions and the overall effects of lignin infusion into the BC papers.

Materials and methods

Materials

Water-soluble alkali lignin (*TCI America*) and sodium hydroxide (NaOH) (*Fisher Scientific*) were commercially sourced.

BC paper fabrication

BC pellicles were grown in a 30×60 cm^2 tank from a symbiotic culture of bacteria and yeast starter formula (*SCOBY; Joshua Tree Kombucha; USA*). Growth media comprised 0.5 wt% tea leaves (filtered out of media before culture began) and 5 wt% of sucrose per liter of water. A single pellicle was harvested after 14 days of incubation, washed with water, and then soaked in a 1 M NaOH solution overnight to remove the embedded bacteria and yeast. The final BC pellicles, after extensive washing with deionized water, were divided into 10×10 cm^2 sheets. Each sheet was placed between water mats (*New Pig Corp.; Tipton, PA, USA*) and metal plates and passed through a metal roller once, before being air dried under a paperweight (~5 kg) for 7 days. Finally, each dried sheet was subjected to hot-pressing following a design of experiment mentioned below. The processing steps are summarized in Fig. 1.

Lignin impregnation

A 0.1 g/mL lignin solution was prepared by dissolving sulfonated alkali lignin in water, stirring under ambient temperature. BC sheets were placed in the solution and stirred at 120 rpm for 1 h before being removed. The resulting lignocellulose (LBC) sheets were placed on a water mat for 3 min on each side to remove excess lignin solution, and subsequently rolled and processed as described above. After the papers were pressed into sheets as described in the following section, a Klason analysis was performed, measuring 15.1 ± 1.9 wt% ($n = 6$) of lignin in the composites.

Design of experiment

BC and LBC sheets were processed under the same design of experiment (DOE) conditions. All samples were initially cold-pressed at 40°C for 5 min at 5 MPa before being hot-pressed. Hot-pressing conditions varied in temperature (120–160°C), pressure (5–15 MPa), and time under pressure (10–30 min). Parameter combinations were assigned in a Latin squares design (See Table S1). A longhand notation is used here where "temperature (°C)/pressure (MPa)/time (min)" is used to refer to the factor-levels of the DOE sample (e.g., "120/5/10" refers to DOE 1, which shares the same factor-levels).

Property-parameter dependence was determined using the Minitab software (Minitab, LLC; State College, PA). A general factorial regression model was fitted to the data for main effects and two-way interactions analyses. For statistically significant main effects ($p < 0.05$) a post hoc Games-Howell analysis at 95% confidence was conducted with one-way ANOVA for further pairwise difference comparisons. Lack-of-fit error analysis was used to determine whether a main effects model was appropriate for the data: a significant value ($p < 0.05$) indicated that the main effects model did not fit the data.

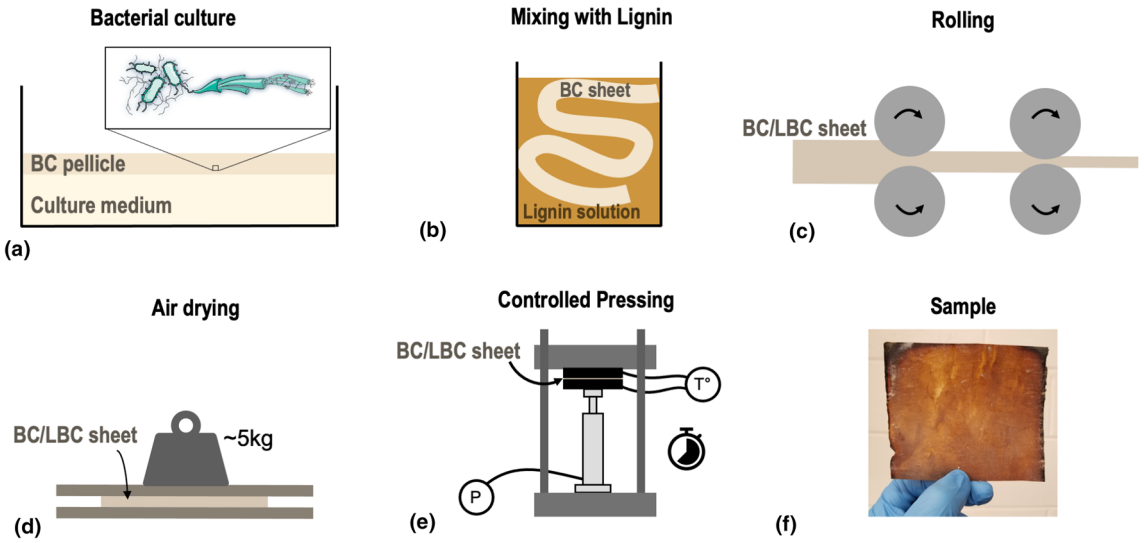

Figure 1. Schematic of bacterial cellulose (BC) sheet processing. (a) BC is cultured in a tank as a pellicle and then cut into smaller sheets. (b) Optional processing step of impregnating BC with lignin via stirring in a dissolved lignin solution. (c) Sheets are rolled out in one direction to remove water and help align fibrils. (d) Sheets are dried under weight until paper-like in thickness and touch. (e) Cold-pressing followed by hot-pressing of sheets under DOE conditions of a specified temperature, pressure, and time. (f) Representative image of a resultant composite sample after processing.

Characterization methods

Scanning electron microscopy (SEM)

Samples were mounted with carbon tape and sputter coated with 4 nm of platinum on an EM ACE600 (Leica Microsystems GmbH; Wetzlar, Germany). SEM imaging was performed on an Apreo VP (ThermoFisher Scientific; Waltham, MA, USA) with an accelerating voltage of 2 kV and 13 pA using a mixed detector mode of T1 (BSE): T2 (SE) at 50:50.

Mechanical testing

Tensile testing was conducted on a mechanical test frame (AGS-X; Shimadzu Scientific Instruments; Columbia, MD, USA) using stock tensile grips with a 5 kN load cell. The tensile testing strain rate was 0.5%/s, adjusted accordingly for each sample. All samples were desiccated for 24 h in a 0% relative humidity chamber before being tested.

Water contact angle

Contact angle tests were performed using a Krüss Drop Shape Analyzer and its processing software, ADVANCE (KRÜSS Scientific; Germany), equipped with a high-resolution CCD camera. This analysis was performed in ambient conditions. Five separate droplets of 4 µL of DI water were placed on each sample after mechanical testing and measured every 15 s for 2 min. The contact angle was determined according to the average angle between the baseline (sample surface) and the left and right tangent (ellipse fit) of a droplet edge.

Stylus profilometry

Surface roughness was measured on a Dektak XTL Stylus Profilometer utilizing Vision64 analysis software (Bruker; Germany). A representative sample from each BC and LBC paper was measured in the parallel and perpendicular directions to the axis of tensile testing (measurement length: 1000 µm, duration: 10 s, force: 3 mg) and the average surface roughness (P_a) was recorded.

X-ray diffraction (XRD)

Diffraction measurements were performed on a D8 Advance (Bruker; Germany) equipped with a Cu Kα source operated at 40 V and 40 A with a wavelength of 1.54184 Å. Samples were laid out on a puck with the direction of testing going along the direction of incident scattering. The degree of crystallinity was calculated using the peak height ratio, after a baseline subtraction, described by Park et al.[14]

Thermogravimetric analysis (TGA)

Thermogravimetric Analysis (TGA) was performed on a Discovery TGA (TA Instruments; New Castle, DE, USA). 2–5 mg of sample was placed in a platinum pan and heated from room temperature to 900°C at 20°C/min in N_2 atmosphere.

Results and discussion

Effects of lignin in BC

Prior work has indicated that lignin may improve binding between cellulose fibrils in a cellulose matrix.[4,5,9,10] In Fig. 2(a) we present the results of tensile testing of all the BC and LBC papers (prepared under the conditions reported in Table S1). Overall, the incorporation of ~15 wt% lignin leads to LBC composites with significantly improved elastic modulus, and marginally improved strength, at the expense of toughness. There are 66% and 9% increases in Young's modulus (E; 9.9 to 16.4 GPa) and ultimate tensile strength (UTS; 128.0 to 139.6 MPa), respectively, and a 58% decrease in toughness (Tgh; 2.48 to 1.04 MJ/m^3) in the lignin-containing composites. The average density for all LBC samples was 1.38 g/cm^3 compared to 1.04 g/cm^3 for BC samples.

Starred values, indicating specific properties, were normalized against individual sample densities and then averaged. Comparing normalized values between the BC and LBC samples confirms the observed positive influence of lignin in the Young's modulus and its reduction of the toughness of the produced papers. Analyzing the specific UTS (UTS*), we observe a marginal strength reduction in the LBC composites compared to BC, though the standard deviations in both cases (UTS and UTS*) overlap.

SEM analysis shows the morphology of pressed BC papers as layered sheets of cellulose fibers [Fig. 2(c)]. The addition of lignin does not fundamentally change this structure at the level of lignin incorporation studied here, as seen in Fig. 2(d). Cross-sectional views of the fracture surface indicate the individual cellulose fibrils as the load-bearing element in both BC and LBC papers, with no distinct lignin phase appearing at the fracture surface of the composite [Fig. 2(c) inset]. The increased stiffness seen in LBC samples suggests that the lignin is well-incorporated into the matrix and mediates binding between cellulose fibrils. However, the decrease in LBC UTS* suggests that lignin acts as an origin for tensile failure, possibly due to the formation of weak, intralayer aggregates. A reduction in strength is seen in other lignin-cellulose materials where they describe the reduced hydrogen bonding from the higher lignin concentrations leading to weaker dry samples.[15] Such aggregates may prevent cracks from reaching the individual cellulose fibrils, thus promoting stress concentration in the weaker lignin-rich areas. Furthermore, lignin does not contribute ductility to BC, as indicated by the brittle failure at UTS in representative stress–strain curves [Fig. 2(b)]. Elongation to break (EtB, equivalent to EtB*) showed a modest difference between BC and LBC: 3% vs. 1%. This decrease could be explained by the hindrance of cellulose chain sliding caused by hardened lignin interfaces between fibrils. The various processing conditions appear to have no significant effect on the crystallinity of the cellulose, as measured by XRD (BC: 82.0 ± 1.8%; LBC: 82.7 ± 0.7%) (See Fig. S1). The incorporation of lignin into the BC matrix also showed no enhancement in thermal stability, as seen from the mass loss profiles of the TGA plots (Fig. S2). In

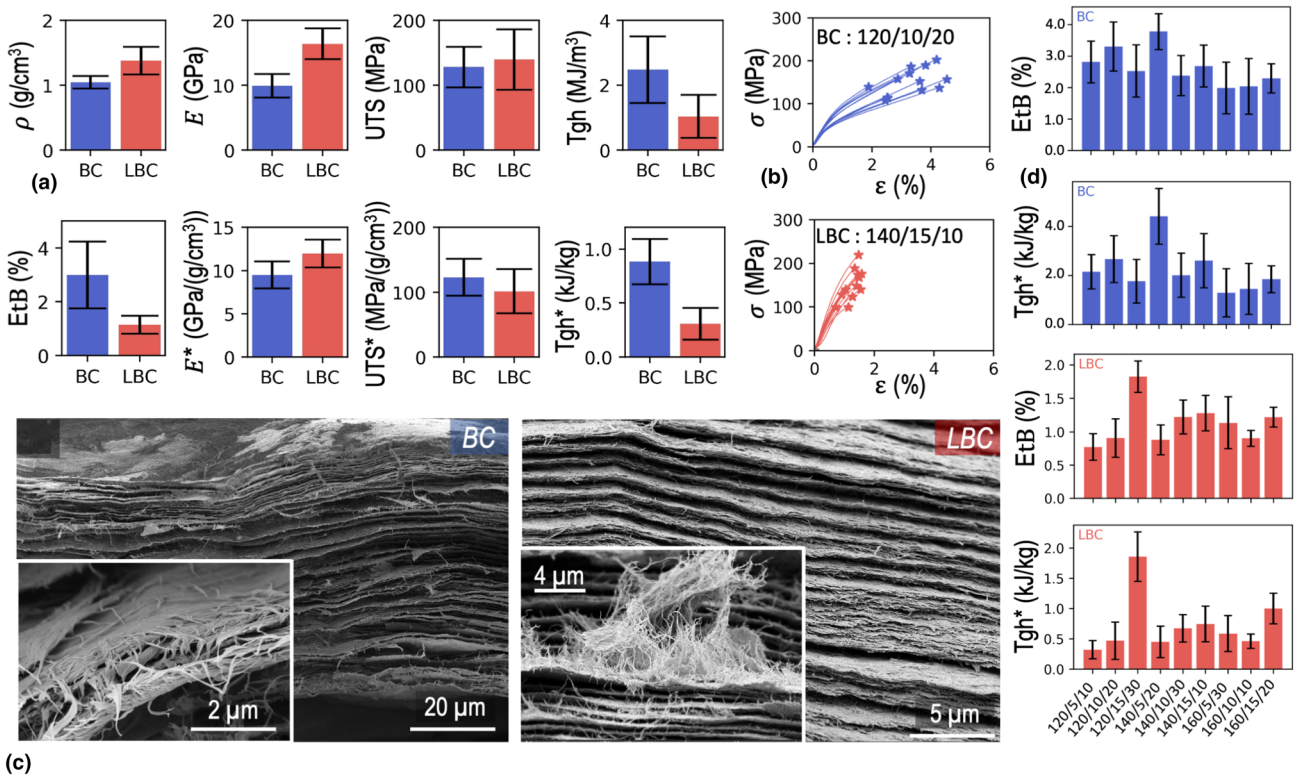

Figure 2. Mechanical properties of BC (blue) and LBC (red) papers. Starred values indicate properties normalized by sample density. (a) Comparative average properties across all DOEs. ρ is density, EtB is elongation to break, E is Young's modulus, UTS is ultimate tensile strength, and Tgh is toughness. The starred properties are normalized to sample density. (b) Representative stress–strain curves for a BC and LBC sample. (c) SEM images depicting the layered structure of the BC and LBC papers at the fracture surface. Insets show individual cellulose fibrils as the primary load-bearing element in these systems. The BC paper is pressed at 160/5/30, and the LBC at 140/5/20. (d) Comparative bar graphs of each DOE condition in BC and LBC for elongation to break and specific toughness. Due to the brittle nature of the samples, EtB has proportional behavior to Tgh*.

fact, the onset of degradation of LBC samples was consistently lower than that of the BC samples. This may be indicative of a low extent of lignin curing in the LBC composites.

DOE analysis of the effects of pressing temperature, pressure, and time on the produced papers

To maximize the mechanical properties and minimize property trade-offs from the introduction of lignin, we investigated the effect of temperature, pressure, and time during the hot-pressing step on the tensile properties of our materials. We hypothesized that these three factors could alter the extent of densification, as well as lignin-cellulose interactions, as prior literature reports demonstrated that hot-pressing temperature alone (around the established transition temperature of lignin, i.e., 80–150°C) indeed allows tuning of the crosslinking and interactions between cellulose and lignin.[9] Each factor was divided into low, medium, and high values (levels) for a design of experiment (DOE, for value ranges see Methods and Table S1). All the measured mechanical properties for each processing condition are found in Figs. S3 and S4.

A Latin squares design minimizes the number of necessary combination of experiments required to infer parameter-property relationships, but all main effects are convoluted with interaction effects as a result.[16] Thus, main effects must be analyzed with potential interactions to be able to draw conclusions. Main effects plots based on a factorial regression model (see Methods) were generated and are summarized in Fig. S5. The regression model assumed no interaction parameters; i.e., all response variation could be explained by a linear combination of each factor-level pair. The one-way ANOVA lack-of-fit errors indicated that this model was appropriately applied for all four specific mechanical responses (E*, UTS*, EtB, Tgh*) for BC samples and EtB for LBC ($p > 0.05$). However, $p < 0.05$ for LBC E*, UTS*, and Tgh* suggested that interactions play a prominent role in these property responses, or that the responses would have a best fit by nonlinear models. p-values from the model ANOVA were used to evaluate whether any of the means at each level were significantly different from each other. Significantly different means were further analyzed using a post hoc Games-Howell test to distinguish the main effect(s) in a sample. Main effects that were significant and resulted in a maximum or minimum for properties are reported in Table S2.

Overall, there were no main effects found to consistently alter the mechanical properties of both BC and LBC samples. In BC, time and temperature were shown to have a significant effect on the final mechanical properties, while pressure did not. The prominent effects of temperature and time are anticipated, as they would directly affect the amount of bound water in the BC papers.[13,17] In fact, molecular dynamics simulations have shown that the inter-fibrillar bound water molecules will spontaneously leave their confinement at temperatures around 160°C,[17] which upon cooling would lead to differences in the degree of inter-fibrillar interactions within the BC papers. In LBC, all three factors had a level showing a main effect. For temperature, 140°C resulted in maxima for E*, UTS*, and Tgh* in BC while the same temperature resulted in minima for E* and UTS* in LBC. In contrast, 160°C maximized properties in LBC while minimizing them in BC. For time, 20 and 30 min resulted in the best and worst UTS*, EtB*, and Tgh* in BC, respectively. Pressing times of 30 min and 10 min resulted in the best and worst of the same properties for LBC, while 20 min maximized only E*.

Conclusions from these main effects can only be drawn in the context of the interactions between our selected processing conditions, which are not accounted for in the main effects plots. Figure S6 depicts the qualitative two-way interaction plots to elucidate the coupled effects of processing conditions in the final mechanical properties of our materials. For example, no pressure–time dependence could be discerned for BC. Pressure had no main effect in BC, so the values of the interaction plots should be proportional to time. Observing the time-pressure interaction plots, in general, 20 min maximizes and 30 min minimizes the UTS*, EtB, and Tgh* as anticipated from the main effects results stated earlier.

Lack-of-fit errors relate to the fit of a linear model. A linear model can inform whether a positive effect on performance is supported or attenuated by another factor. If a factor-level increases the performance of a material in a linear system, then we can be reasonably certain that factor-level alone is the reason for the improvement. To validate the lack-of-fit error analysis, we can take combinations of the extrema of performances from the main effects and compare against the DOE that corresponds to their two-way interactions. For a linear main effects model, the performances of combined main effects are equivalent to that of interaction pairs, since interactions effects are small or nonexistent. That is, the average of two main effect properties should be similar to the same two-way interaction's properties. In contrast, if interactions are strong and a main effects model does not fit, the theoretical combination of two main effects may not be the same as the actual properties of a two- way interaction. The properties for which main effects of BC exist and can be compared against its two-way interactions are UTS*, EtB, Tgh*. Specifically, we compare a combination of temperature and time since there are no main effects for pressure. The factor-levels that produced the highest, lowest, and a combination of the highest and lowest main effects are plotted in Fig. S7. From these values, we can tell if the linear model is correct based on how close the DOE and main effect combinations are to each other. In all cases, the properties of the mixed values lie between that of the extrema. Furthermore, the values of the DOE and predicted main effects are close, with an average percent difference of 10% (UTS*), 24% (Tgh*), and 14% (EtB). These small differences suggest that interaction effects, if present, are small in the BC papers.

Due to the possibility of three-way interactions in LBC papers, paired combinations of all three factors were analyzed (Fig. S8). In these cases, the mixed main effects all fell between the high and low values. However, the mixed DOE properties did not consistently fall between these values, and their positive or negative deviations could not be predicted by the values of the main effect combinations. Compared to the BC UTS* temperature–time interaction, the equivalent for LBC showed a larger average percent difference between the DOE and main effects values (BC 10% vs. LBC 18%), again supporting that the linear main effects model does not apply for LBC because interactions are significant. Temperature–time and temperature–pressure appeared to have the largest interactions in LBC papers, based on the relative deviations of the measured mechanical properties to the theoretical main effects combination properties.

Structure-processing-property relationships

Our DOE analysis revealed that interactions between our processing parameters (pressure, time, temperature) possibly influence the mechanical properties of the LBC composites, while temperature–time and temperature–pressure have synergistic effects. The combination of temperature and time may affect the degree or kinetics of lignin curing and crosslinking or adhesion to cellulose fibrils,[9] while temperature and pressure may be involved with the degree to which deeper-penetrating lignin particles are cured. SEM analysis was conducted on BC and LBC samples to investigate further microstructural differences in response to the processing conditions (Fig. 3). A common observation across all samples, was the formation of defects from the rolling process, evidenced by parallel sheets folding back onto themselves, seen at low magnification [Fig. 3(a)]. Under low temperature pressure and intermediate time (120/10/20), we observe discrete lignin particles present in deeper layers of an LBC sample [Fig. 3(b)], demonstrating that not all lignin was cured evenly throughout the sample during processing. In agreement with this observation, the lowest temperature, pressure, and time conditions (120/5/10 and 120/10/20) produced the LBC composites with lowest UTS*, EtB, and Tgh*. The pure BC material, before any processing, is formed by the sequential deposition of cellulose fibrils in a thick multilayered arrangement as shown in Fig. 2(c). Each layer (hereafter denoted "plane") is essentially a continuous, porous matrix with discrete cellulose fibrils, which serve as the load-bearing elements. In all the samples (BC and LBC) we observed interplanar fibril bridging [Fig. 3(c)], whereby the fibrils from one plane extended into a neighboring one, acting

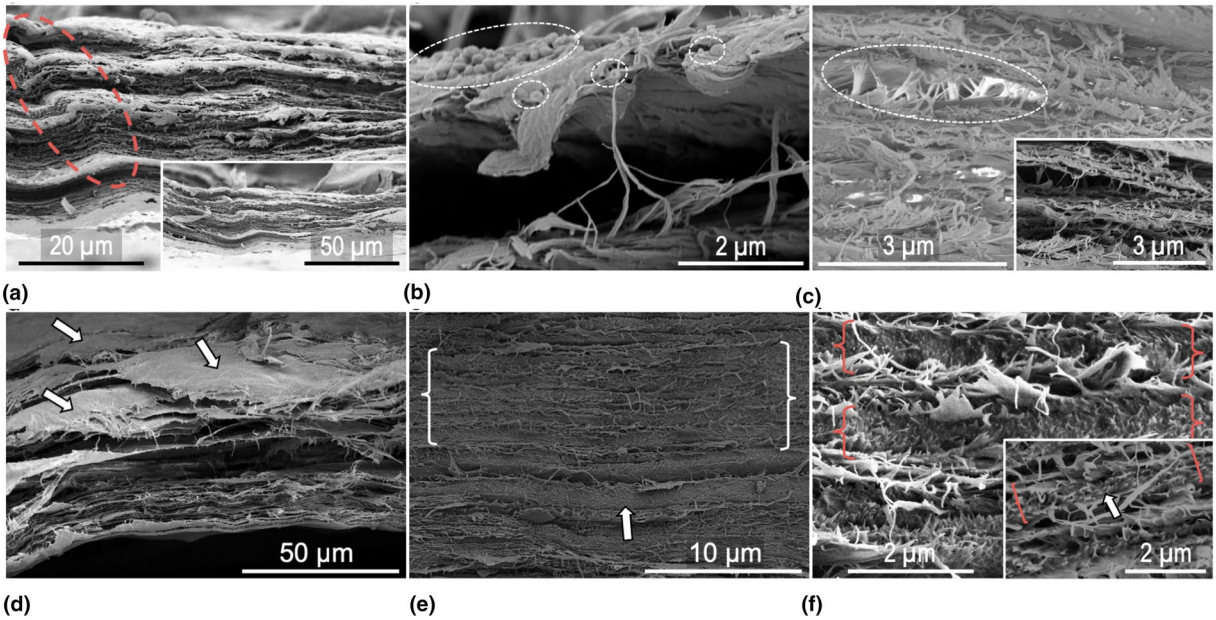

Figure 3. SEM analysis of BC and LBC samples. (a) Low-magnification (×2000), cross-sectional view of BC (160/10/10). A defect is highlighted in which the sheet rolls back onto itself due to rolling process before controlled pressing. Inset: A ×1000 view of the defect and BC sheet. (b) Uncured, round lignin particles on top of BC fibrils and layers (from 120/10/20). (c) Interlayer binding fibrils highlighted. Inset: The same image in another detector mode to highlight planes and the spacings between them. (LBC sample from 120/5/10) (d) Top and cross-sectional view of a BC sheet showing both amorphized sheets (arrows) and sheets made of discrete fibrils. (BC sample from 120/5/10) (e) An LBC sample (160/5/30; ×5000 magnification) with stacked lignin-BC composite planes in brackets. The arrow points at a single composite plane instance. (f) A magnified image of (e; ×20,000) highlighting the composite planes and the spacing between each plane. The inset depicts a ×50,000 magnification to highlight fused and fractured lignin-BC fibrils.

as a primary strengthening mechanism in agreement to prior literature observations.[3,17,18]

As a result of our processing conditions, we found, in addition to the above, the formation of amorphized sheets, consisting of fused, indistinguishable cellulose fibrils [Fig. 3(d)]. We speculate that the fibrils fused together during processing due to cellulose layer interactions under elevated temperature–time–pressure conditions, and that the presence of extensive amorphized sheets would hinder individual fibril sliding as a deformation mechanism. From the mechanical property results (Fig. S4, SI), we saw that BC samples pressed at 160°C have the lowest average EtB and Tgh* compared to any of the other pressing conditions, regardless of the time. At 30 min of pressing time, the samples pressed at 120 and 140°C have the second lowest EtB and Tgh*. SEM images show the formation of substantially more amorphized layers in these samples that show minimized toughness and EtB [Fig. 3(d)]. On the other hand, the lowest temperatures (120 and 140°C) at the lower pressing times had the highest Tgh* and EtB. These results indicate that (i) temperature was the primary contributor to amorphization but required an adequate amount of time to optimize the extent of amorphization, and (ii) extensive amorphized layers restricted chain mobility, thus causing reductions in toughness and EtB. In the composite papers, SEM images revealed an additional plane element, which consisted of the base porous cellulose matrix plane densified by the penetration and curing of lignin to form a lignin-BC composite [Fig. 3(e)–(f)]. These composite planes showed no distinct interfaces between the lignin filler and cellulose matrix due to the space-filling properties of the solubilized lignin before curing. The mechanical property results [Fig. 2(a), S3, and S4] support further the excellent adhesion between the composite components. As in the case of the amorphized sheets, fibril sliding would be impeded in presence of the lignin binder, at least until failure of the binder. Indeed, we observe a higher average E and E* of LBC compared to BC [Fig. 2(a)], supporting that in the elastic regime, before any plastic deformation of lignin or cellulose, the presence of lignin improves binding between adjacent cellulose fibrils to more evenly distribute load.

The best performing samples for pure BC depended on the property of interest, with 140/15/10 having the greatest E* and 140/5/20 and 140/15/10 being the top performers in UTS*, EtB, and Tgh*. The intermediate temperature causing the best properties suggests that there is a temperature threshold differentiating the effects of amorphization. At that threshold (140°C), the formation of localized amorphized areas begins, and the samples see positive effects in their stiffness, strength, and toughness, possibly due to enhanced intralayer interactions, while the interplanar fibril bonding is not yet hindered. As processing temperature and time increase (140/10/30, and all 160°C conditions), the amorphized areas could dominate the performance, hindering long-range fibril interactions and effectively reducing strength, stiffness, and toughness, which is

what our mechanical testing results show. In addition, at those conditions thermal degradation may start to occur, contributing to mechanical property deterioration.

Regarding the LBC composites, the best performance in any of the mechanical properties consistently came from conditions 120/15/30, 140/15/10, and 160/15/20. As concluded from the DOE analysis presented in the previous section, the performance of the LBC composites is highly dependent on the interactions between the processing factors, rather than on a single factor. We note, however, that the composites with minimum strength and toughness are those formed at the lowest temperature, time, and pressure levels (120/5/10 and 120/10/20), which also presented uncured lignin particles in SEM [Fig. 3(b)]. When comparing the performance of LBC composites to that of pure BC processed at 120°C, we see that lignin caused a substantial increase in the modulus, with no effect in strength and an overall reduction in EtB and toughness. Yet at the longest pressing time at that temperature (120/15/30) the stiffness, strength, and toughness are all improved in the presence of lignin. Therefore, lignin curing can improve the overall mechanical properties of composites below the amorphization threshold conditions we observed for the pure BC.

Effects of lignin on the wetting behavior of the composites

Natural lignin is known to promote water hydrophobicity in wood and therefore minimize swelling that could structurally degrade wood. However, the extraction and processing of lignin from woody biomass significantly impact the water properties (solubility and hydrophobicity) of lignin products through changes in the molecular weight and the degree of sulfonation.[19] We conducted water droplet tests to measure the effects of processed, sulfonated (water-soluble) lignin in our composites. By utilizing a combination of a 3-parameter decay function and the Avrami model proposed by Farris et al.,[20] water absorption properties were further analyzed. Contact angle measurements were taken over a period of 2 min, allowing for the differentiation between water absorption versus spreading. These two phenomena are assumed to occur simultaneously.

Here, the parameters k and n represent the contact angle evolution rate and the relative fraction of absorption versus spreading (0 = pure absorption, 1 = pure spreading), respectively. Compared to the strongest BC sample (140/5/20), the weakest BC (160/5/30) had a higher immediate contact angle (83.7° vs 76.5°) but showed more absorption of water at a significantly faster rate [seen in Fig. 4(a), (b)]. The strongest

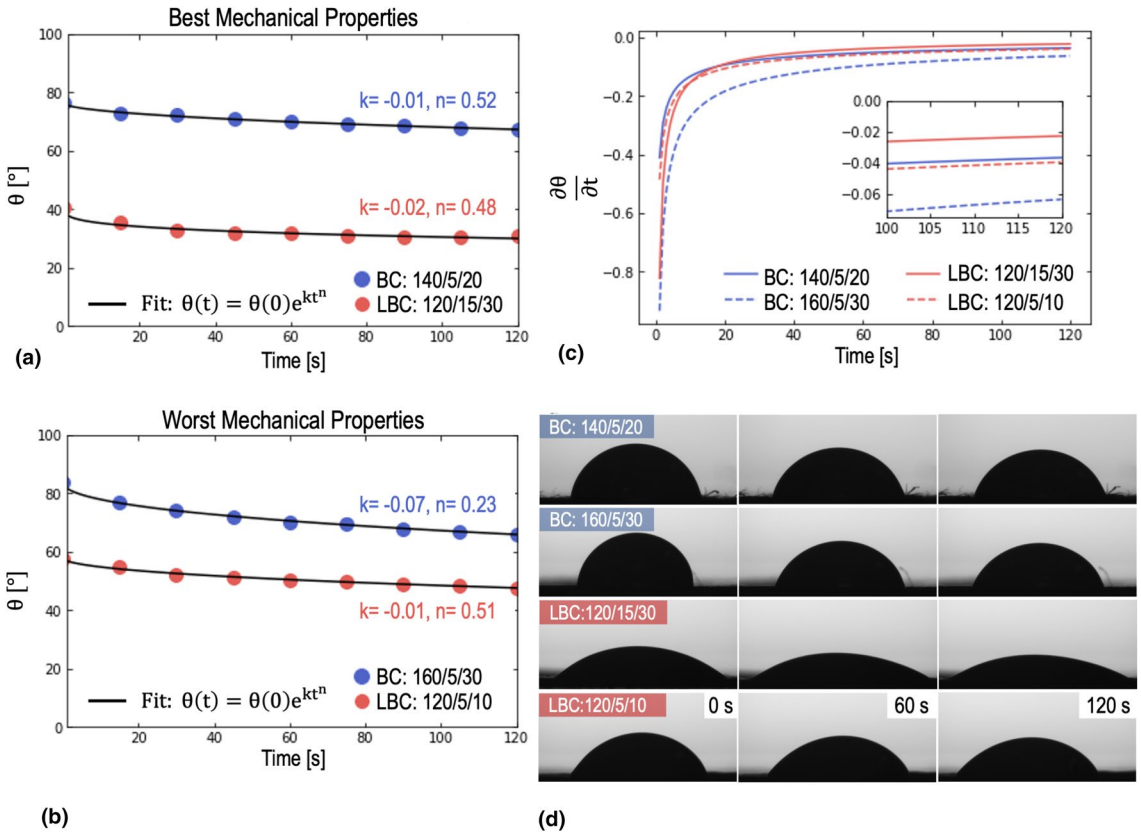

Figure 4. Water absorption in BC (blue) and LBC (red). (a) Time-dependent contact angle and fitted curve for the best mechanically performing BC and LBC sheets. (b) Time-dependent contact angle and fitted curve for the worst mechanically performing BC and LBC sheets. (c) First derivative of the fitted data with inset magnifying the last 20 s. (d) Images of water droplets at 60 s time intervals.

lignin composite (120/15/30) had a lower immediate contact angle compared to the weakest (120/5/10) (40.7° vs. 57.8°) but showed roughly equal absorption and spreading between the two samples, demonstrating that processing conditions do not affect the long-term water resistance in the composites. The results show that the incorporation of lignin imparts hydrophilicity on the material, as evidenced by the lower contact angle values, which is justified from the use of water-soluble lignin in these composites.[19] As discussed above, SEM images revealed uncured lignin particles in the composite with weakest mechanical properties [Fig. 3(b)], while the strongest composites had a continuous lignin-infused matrix. Given the hydrophilicity of our lignin, the lower contact angle for the composite with more even lignin spreading (strongest sample) is justified.

Of the four-studied samples, the strongest and weakest LBC have a similar average P_a of 4.4 ± 2.4 μm and 4.4 ± 2.0 μm, respectively. In contrast, the strongest and weakest BC have a P_a of 3.7 ± 0.4 μm and 6.8 ± 3.2 μm, respectively. This result confirms the hypothesis that the highest surface roughness (weakest BC, $k = -0.07$, $n = 0.23$) displays the greatest water absorption over time, and highest initial hydrophobicity (at $t = 0$ s). By the end of two minutes, there is still absorption and spreading of water occurring, most prominently in the weakest BC sample. This observation is emphasized by the first derivative of the contact angle over time (generated from the fitted data, Fig. 4(c)). While none of the samples reached the zero-speed rate within the two-minute time frame, the weakest BC sample starts and continues to wet the fastest. Snapshots of the water droplets at 0 s, 60 s, and 120 s are compared in Fig. 4(d).

Conclusion

In this work, we present the effects of incorporating lignin in bacterial cellulose matrices and analyze how altering processing (cold- and hot-pressing) temperature, pressure, and time conditions allow tuning of the mechanical properties in the resultant composite papers. Infiltrating lignin in the unique layered cellulose matrix we explore here comes with property trade-offs; it induces a significant improvement in stiffness, but also creates new sources of defects for brittle failure. Our results demonstrate that there is a temperature–pressure and temperature–time threshold above which lignin penetration into and incorporation in the dense BC structure is optimized to form a continuous composite matrix with enhanced stiffness, strength, and toughness compared to the base BC matrix. Below that threshold, lignin particles are not able to infuse into the BC matrix, causing an enhancement to only the Young's modulus while reducing improvements to strength and toughness. In addition, we report a cellulose amorphization mechanism controlling the mechanical behavior of pure BC materials in response to the processing conditions. We notice that when the processing temperature and time are intermediate (140°C) the formation of amorphized intralayer areas, in which cellulose fibrils are fused together, enables an improved strength, modulus, and toughness. However, at higher temperatures and processing times, the possible cellulose degradation as well as the enlargement of amorphized layers, which hinders discrete intra- and inter-layer fibrillar interactions, effectively reduce the strength and toughness of the pure BC papers. Finally, we investigated the effects of processing on our nanopaper hydrophobicity, given that lignin confers hydrophobic properties in nature. We found that the same solubility that allows lignin to infiltrate the BC matrix and improve mechanical properties caused the BC matrix to become more hydrophilic. That is, the lignin in the best mechanically performing sample was better integrated throughout the matrix, causing greater absorption and spreading of water initially and over time. The opposite behavior was found for the worst mechanically performing sample, implying that lignin was less well incorporated and distributed in the BC. Our results demonstrate how introducing lignin and varying processing conditions allow different mechanical and water properties to be achieved in BC papers.

Acknowledgments

The authors thank Jeff Hsu, Danielle Uchimura Pascoli, and Prof. Renata Bura for their generous time and resources in conducting the Klason analysis of our composite materials. We also thank Hareesh Iyer for his supporting work with tensile testing and statistical analysis. Part of this work was conducted at the Molecular Analysis Facility, a National Nanotechnology Coordinated Infrastructure (NNCI) site at the University of Washington, which is supported in part by funds from the National Science Foundation (awards NNCI-2025489, NNCI-1542101), the Molecular Engineering and Sciences Institute, and the Clean Energy Institute. The authors are also grateful for the support of the Washington Clean Energy Testbeds (WCET).

Data availability

The data generated and presented in this study are available from the corresponding author on reasonable request.

Declarations

Conflict of interest

The authors declare no conflicts of interest.

Supplementary Information

The online version contains supplementary material available at https://doi.org/10.1557/s43579-022-00191-8.

References

1. R.J. Moon, A. Martini, J. Nairn, J. Simonsen, J. Youngblood, Cellulose nanomaterials review: structure, properties and nanocomposites. Chem. Soc. Rev. **40**, 3941–3994 (2011). https://doi.org/10.1039/c0cs00108b
2. T. Li, C. Chen, A.H. Brozena, J. Zhu, L. Xu, C. Driemeier, J. Dai, O.J. Rojas, A. Isogai, L. Wågberg, others: developing fibrillated cellulose as a sustainable technological material. Nature **590**, 47–56 (2021)

3. Q. Meng, T.J. Wang, Mechanics of strong and tough cellulose nanopaper. Appl. Mech. Rev. **71**, 040801 (2019)
4. X. Wang, Q. Xia, S. Jing, C. Li, Q. Chen, B. Chen, Z. Pang, B. Jiang, W. Gan, G. Chen, M. Cui, L. Hu, T. Li, Strong, hydrostable, and degradable straws based on cellulose-lignin reinforced composites. Small **17**, 2008011 (2021). https://doi.org/10.1002/smll.202008011
5. Q. Xia, C. Chen, Y. Yao, J. Li, S. He, Y. Zhou, T. Li, X. Pan, Y. Yao, L. Hu, A strong, biodegradable and recyclable lignocellulosic bioplastic. Nat. Sustain. **4**, 627–635 (2021). https://doi.org/10.1038/s41893-021-00702-w
6. C. Chen, Y. Kuang, S. Zhu, I. Burgert, T. Keplinger, A. Gong, T. Li, L. Berglund, S.J. Eichhorn, L. Hu, Structure–property–function relationships of natural and engineered wood. Nat. Rev. Mater. **5**, 642–666 (2020). https://doi.org/10.1038/s41578-020-0195-z
7. E.J. Foster, R.J. Moon, U.P. Agarwal, M.J. Bortner, J. Bras, S. Camarero-Espinosa, K.J. Chan, M.J. Clift, E.D. Cranston, S.J. Eichhorn, Current characterization methods for cellulose nanomaterials. Chem. Soc. Rev. **47**, 2609–2679 (2018)
8. R.Y. Yeap, *The Potential of Lignin to Increase the Hydrophobicity of Micro/Nanofibrillated Cellulose (MNFC)* (2020)
9. B. Jiang, C. Chen, Z. Liang, S. He, Y. Kuang, J. Song, R. Mi, G. Chen, M. Jiao, L. Hu, Lignin as a wood-inspired binder enabled strong, water stable, and biodegradable paper for plastic replacement. Adv. Funct. Mater. **30**, 1906307 (2020). https://doi.org/10.1002/adfm.201906307
10. M. Farooq, T. Zou, G. Riviere, M.H. Sipponen, M. Österberg, Strong, ductile, and waterproof cellulose nanofibril composite films with colloidal lignin particles. Biomacromol **20**, 693–704 (2019). https://doi.org/10.1021/acs.biomac.8b01364
11. J. Song, C. Chen, S. Zhu, M. Zhu, J. Dai, U. Ray, Y. Li, Y. Kuang, Y. Li, N. Quispe, Y. Yao, A. Gong, U.H. Leiste, H.A. Bruck, J.Y. Zhu, A. Vellore, H. Li, M.L. Minus, Z. Jia, A. Martini, T. Li, L. Hu, Processing bulk natural wood into a high-performance structural material. Nature **554**, 224–228 (2018). https://doi.org/10.1038/nature25476
12. R. Mao, S. Goutianos, W. Tu, N. Meng, G. Yang, L.A. Berglund, T. Peijs, Comparison of fracture properties of cellulose nanopaper, printing paper and buckypaper. J. Mater. Sci. **52**, 9508–9519 (2017)
13. S. Wang, F. Jiang, X. Xu, Y. Kuang, K. Fu, E. Hitz, L. Hu, Super-strong, super-stiff macrofibers with aligned, long bacterial cellulose nanofibers. Adv. Mater. **29**, 1702498 (2017). https://doi.org/10.1002/adma.201702498
14. S. Park, J.O. Baker, M.E. Himmel, P.A. Parilla, D.K. Johnson, Cellulose crystallinity index: measurement techniques and their impact on interpreting cellulase performance. Biotechnol. Biofuels **3**, 1–10 (2010). https://doi.org/10.1186/1754-6834-3-10/TABLES/2
15. J. Wang, W. Chen, T. Dong, H. Wang, S. Si, X. Li, Enabled cellulose nanopaper with outstanding water stability and wet strength via activated residual lignin as a reinforcement. Green Chem. **23**, 10062–10070 (2021). https://doi.org/10.1039/D1GC03906G
16. R. Kohli, Assessing interaction effects in Latin square-type designs. Int. J. Res. Mark. **5**, 25–37 (1988). https://doi.org/10.1016/0167-8116(88)90014-6
17. M. Wohlert, T. Benselfelt, L. Wågberg, I. Furó, L.A. Berglund, J. Wohlert, Cellulose and the role of hydrogen bonds: not in charge of everything. Cellulose **29**, 1–23 (2021)
18. A.J. Benítez, J. Torres-Rendon, M. Poutanen, A. Walther, Humidity and multiscale structure govern mechanical properties and deformation modes in films of native cellulose nanofibrils. Biomacromol **14**, 4497–4506 (2013). https://doi.org/10.1021/bm401451m
19. T. Aro, P. Fatehi, Production and application of lignosulfonates and sulfonated lignin. Chemsuschem **10**, 1861–1877 (2017). https://doi.org/10.1002/cssc.201700082
20. S. Farris, L. Introzzi, P. Biagioni, T. Holz, A. Schiraldi, L. Piergiovanni, Wetting of biopolymer coatings: contact angle kinetics and image analysis investigation. Langmuir **27**, 7563–7574 (2011). https://doi.org/10.1021/LA2017006/SUPPL_FILE/LA2017006_SI_001.PDF